

Article

Spatiotemporal Conflict Analysis and Prediction of Long Time Series Land Cover Changes in the Black Soil Region of Northeast China Using Remote Sensing and GIS

Ding Ma, Sijia Jiang, Xin Tan, Mingyu Yang, Qingbin Jiao and Liang Xu *

Changchun Institute of Optics, Fine Mechanics and Physics, Chinese Academy of Sciences, Changchun 130033, China; mading@ciomp.ac.cn (D.M.)

* Correspondence: xuliang@ciomp.ac.cn; Tel.: +86-136-9430-8084

Abstract: Using remote sensing and GIS techniques to monitor long time series land cover changes is of great significance to understanding the impact of human activities on spatiotemporal conflicts and changes in cropland and forest ecosystems in the black soil region of Northeast China. Spatial analysis and dynamic degree were used to analyze the evolutionary process and spatiotemporal association of land cover from 1990 to 2020; the transfer matrix was used to analyze and reveal dynamic conversions of land cover from 1990 to 2000, 2000 to 2010, and 2010 to 2020; and the GM (1,1) model was used to forecast the changes in land cover by 2025 based on historical data. The results indicated that the dominance of forest and cropland did not change from 1990 to 2020, and the average area of forest and cropland was 512,713 km² and 486,322 km², respectively. The mutual conversion between cropland, forest, grassland, and bare areas was the most frequent. The area of cropland converted into forest and grassland was 14,167 km² and 25,217 km², respectively, and the area of forest and grassland converted into cropland was 27,682 km² and 23,764 km², respectively, from 1990 to 2000. A similar law of land cover change was also presented from 2000 to 2020. In addition, the predicted values of cropland, forest, grassland, shrubland, wetland, water bodies, impervious surfaces, and bare areas were 466,942 km², 499,950 km², 231,524 km², 1329 km², 11,775 km², 18,453 km², 30,549 km², and 189,973 km², respectively, by 2025. The maximum and minimum residuals between the predicted and actual values were 6241 km² and −156 km² from 1990 to 2020. The evaluation results of the GM (1,1) model showed that all of the evaluation indices were within an acceptable range, and that the posteriori error ratio and class ratio dispersion were both less than 0.25. Through comparison with other studies, this study is not only able to provide some experience for further analyzing the spatial and temporal changes in land cover and its future prediction but also provide a basis for comprehensive management in Northeast China.

Keywords: land cover; long time series; GM (1,1) model; black soil region; spatiotemporal analysis; human activities; Northeast China



Citation: Ma, D.; Jiang, S.; Tan, X.; Yang, M.; Jiao, Q.; Xu, L. Spatiotemporal Conflict Analysis and Prediction of Long Time Series Land Cover Changes in the Black Soil Region of Northeast China Using Remote Sensing and GIS. *ISPRS Int. J. Geo-Inf.* **2023**, *12*, 271. <https://doi.org/10.3390/ijgi12070271>

Academic Editors: Wolfgang Kainz and Godwin Yeboah

Received: 7 April 2023

Revised: 25 June 2023

Accepted: 29 June 2023

Published: 6 July 2023



Copyright: © 2023 by the authors. Licensee MDPI, Basel, Switzerland. This article is an open access article distributed under the terms and conditions of the Creative Commons Attribution (CC BY) license (<https://creativecommons.org/licenses/by/4.0/>).

1. Introduction

Humans have been reshaping the Earth's surface for millennia [1,2]. However, lacking the change information of regional or global time series land cover about millennium ecosystem, which constrains analyzing the consequences of ecosystem change [3–6]. With the increasing focus on sustainability [7,8] and global changes in climate and environment [9–11], the discipline of land change has become an important scientific area for addressing these challenging problems [12–14]. Changes in global land use and land cover have affected the condition and integrity of different ecosystems, giving rise to damage to ecosystem services and functions in recent decades [15–17]. Land change associated with biodiversity loss, deforestation, and soil desertification can be understood through the dynamic evolution of land cover [18–20]. Exploring the structure and dynamics of land cover is also crucial for urban planning and management [21–23], which can guide planners and

managers to promote the development of sustainable urban areas [24,25]. More specifically, the accurate evaluation of the changes in land cover is the basis for studying the evolution mechanisms of ecosystems as well as a significant tool for quantifying the impact of human activities on ecosystems [2,26–28].

With the development of remote sensing (RS) and geographic information system (GIS) technology, the specific applications for land cover change information are many and varied [29–32]. Information on long time series land cover changes provides a reproducible and efficient means of simulating the dynamic scenario of vegetation succession in future forests, cropland, and grassland [33,34]. The National Aeronautics and Space Administration (NASA) and the United States Geological Survey (USGS) jointly initiated Landsat 1 in the early 1970s, which represents the longest collection period of Earth observation satellite data for agriculture, forestry, animal husbandry, and water resources around the world [35,36]. Since 2008, all Landsat data with an invariable spatial resolution and similar spectral bands have been freely available to users. The global Collection 1 data processing (since 1982) includes consistent observation quality analyses and geometric as well as radiometric correction, enabling a multidecade assessment of land cover changes and land use to a large geographical extent [37]. The transfer matrix of land use/land cover can define the important processes of anthropogenic changes to land cover, such as ecological restoration engineering, cultivated land expansion, land degradation, and urbanization [38,39]. Different from land use, land cover focuses on the natural properties of land and can be an important input for climate models of terrestrial ecosystems and natural resources. Land use focuses on the social attributes of land and describes its social, economic, and cultural utility, as well as its ecosystem functions [40–42]. Collectively, these sources allow researchers to make improvements to operational classification and change detection and to draw better inferences about landscapes and inherent processes that are associated with forest destruction and agricultural expansion caused by human activities [43–45].

In recent years, the systematic monitoring of large areas of land cover has become popular, and most researchers assume that the changes in land cover and land use are mainly caused by human activities (including induced environmental changes) [46]. Temgoua et al. analyzed land cover dynamics in the Melap forest reserve in the years 1988, 2000, and 2018 in the west of Cameroon [47]. Faruque et al. used remote sensing and geographic information system techniques to monitor the changes in land cover in the mangrove areas of Bangladesh in 1990, 2000, 2010, and 2020 [48]. Kombate et al. studied the dynamic changes in land cover and forest cover in Togo between 1985 and 2020, and found that forest cover decreased substantially over the most recent 30-year period [49]. Souverijns et al. used Landsat time series data to evaluate the changes in 30 years of land cover in the Sudano-Sahel region, and were able to detect forest degradation resulting from subtle changes [50]. The drivers and implications of land cover dynamics in the Finchaa Catchment, northwestern Ethiopia, were analyzed using Landsat images [51]. By correlating the area of the Lake Victoria Basin from natural vegetation categories to farmland and urban areas and exploring the relationship between these categories of land cover conversion, it can be found that, during the 1985–2014 period, land cover change was mainly driven by human activities, resulting in the conversion of forests, woodland, grassland, and wetland into farmland or settlements [52]. The use of long time series land cover data provided a theoretical basis for promoting ecological sustainable development and environmental decision making in the Yellow River Basin [53], Mongolian Plateau [54], Loess Plateau [55,56], and Tibetan Plateau [57]. Land cover change was also used to monitor long-term desertification changes in the Ternata oasis in the country of Morocco [58]. Thamaga et al. used the Landsat dataset to assess the impact of land cover change on unprotected wetland ecosystems in the arid tropics of South Africa [59]. In particular, the La Plata region had major losses in grassland area from 2000 to 2014, mostly as a result of the expansion of agricultural boundaries [60]. The combination of Landsat and Sentinel-2 sensors has also become an important data option for assessing the changes in land cover

in different countries around the world, such as Germany, Russia, and Poland [61]. Nasiri and Som-ard et al. determined the spectral time index extracted from the satellite time series through the synthesis method of Landsat 8 and Sentinel 2, and generated a land cover map [62,63]. The results showed that Landsat 8 had greater advantages over Sentinel 2 in the monitoring of forests, herbaceous vegetation, and water; the former was more accurate [64]. The use of long time series data also provided opportunities for the forecasting of land cover and desert greening in the future, such as a dynamics of land system (DLS) model [65], land change evaluation model [66], CA-Markov model [44,67,68], and GM (1,1) model [69,70]. Among them, the GM (1,1) model can build mathematical models and make forecasts based on a small amount of incomplete information and data by considering the law of the past and present development of objective things [71]. It is usually used in time series prediction, distortion prediction (disaster prediction), system prediction, and topological prediction (waveform prediction). In particular, it has a unique effect on the analysis and modeling of a system with a short time series, less statistical data, and incomplete information. Compared with a common regression analysis, the GM (1,1) model will not produce a large error in the case of small samples, so it has a wide range of applications in various prediction fields, such as grain consumption, satellite clock bias, and runoff forecasts, and is an effective tool for dealing with the problem of small-sample prediction [72–74].

In addition, some scholars have carried out a series of studies on the black soil region of Northeast China. Northeast China was a significant ecological forest region, accounting for more than 30% of China's total forest area, and the trees were cut down most frequently in this region before 1998 [75]. At the same time, it was also the most important agricultural production region in China, which was one of the three largest black soil regions in the world [76]. Black or dark black humus topsoil is a significant natural resource and is the most fertile soil in the world [77]. The accurate determination of the quantity and spatial distribution of cultivated land in the black soil region of Northeast China is very important for sustainable agricultural development [78]; however, the land exploitation and utilization have been fast and intensive since large-scale agricultural development in 1900, and the land cover has changed significantly in Northeast China [79]. The total area and unit stock of natural forest have decreased sharply because of human activities [80,81]. Since 2021, the national government, together with the Chinese Academy of Sciences and universities, has set up a black soil research demonstration zone in Northeast China and put forward a black soil protection project to protect the sustainable development of black soil. Ye et al. reconstructed the changes in cultivated land cover in Northeast China in the past 300 years by converting literature data and multisource data [82]. Mao et al. assessed the impact of policies on land cover and ecosystem services from 2000 to 2015 by combining remote sensing, meteorological records, and statistical data [83]. Liu et al. analyzed the ecological security pattern and its influences on urban expansion in the black soil agricultural area of Changchun City [84]. Xie et al. combined 300 years of cropland area and national water conservancy survey data to quantitatively analyze the spatial and temporal variations in soil erosion from 1653 to 2012 in Northeast China [85]. Zhu et al. combined a Markov chain model and remote sensing data in 2000, 2005, and 2010 to simulate a land use/cover change structure in Fuyuan City, a black soil region in Northeast China [86]. Wang et al. improved the accuracy of cropland extraction in the black soil region of Lishu County by using multiseason remote sensing images [78]. Zhao et al. also combined multitemporal Landsat images with postclassification strategies to analyze the laws of urbanization, deforestation, and agricultural expansion in Northeast China [75]. Therefore, from the above literature survey, it can be known that it is necessary and urgent to study the internal conversion law of forest, farmland, grassland, and other types of land cover caused by human activities and policies in this region, which is also crucial for understanding the land loss caused by human activities. In particular, there are very few studies on large-area land cover change and its spatiotemporal prediction in recent years with regard to the black soil region of Northeast China.

In summary, the internal conversion among different types of land cover caused by human activities in Northeast China in recent years is still unclear, which is not conducive to the comprehensive management of regional land cover. Thus, the primary aims of this study are as follows: (1) Firstly, we used the remote sensing and GIS techniques to analyze the spatiotemporal changes in and dynamic degree of land cover in Northeast China in the past thirty years (Section 3.1). (2) Secondly, we made attempts to uncover the dynamic conversions of land cover from 1990 to 2000, 2000 to 2010, and 2010 to 2020 (Section 3.2), and used the GM (1,1) model to forecast changes in land cover from 1990 to 2020 based on historical data. (3) Finally, we used the maximum residuals to analyze the differences between predicted and actual values, and used the GM (1,1) model to predict changes in land cover by 2025. The posteriori error ratio, root mean square error, infinitesimal error probability, and class ratio dispersion were calculated to verify the accuracy of the GM (1,1) model (Section 3.3). This research provides some experiences for the further analysis of the spatiotemporal transformation of land cover and its future prediction in the black soil region of Northeast China.

2. Materials and Methods

2.1. Study Area

Northeast China is between $111^{\circ}8' \sim 135^{\circ}5' E$ and $38^{\circ}43' \sim 53^{\circ}33' N$, and includes Liaoning, Jilin, Heilongjiang, and parts of Inner Mongolia Province (Figure 1). The study region covers nearly 1,448,286 km² and an average altitude ranging from 50 to 200 m. It is located in the middle and cold temperate zone, belonging to the temperate monsoon climate zone, which is warm and rainy in summer, while being cold and dry in winter. The annual mean temperature and precipitation are $-20 \sim 25^{\circ} C$ and 300~1000 mm, respectively. It is bounded on the south by the Yellow River and the Bohai Sea, on the east and north by the Yalu River, the Tumen River, the Ussuri River, and the Heilongjiang River, and on the west by Mongolia and Russia. The inner part is the high mountains, middle mountains, low mountains, and hills of the Greater Khingan Mountains, Lesser Khingan Mountains, and Changbai Mountains, and the central part is the Northeast Plain. The total area of the Northeast Plain, which can be divided into the Songnen Plain, Liaohe Plain, and Sanjiang Plain, is almost equal to the mountain area. The land area suitable for reclamation in Northeast China is about 666,667 km², mainly rich in rice, corn, soybean, potatoes, sugar beet, sorghum, and temperate fruits and vegetables. Animal husbandry is the main industry in the eastern Inner Mongolia Autonomous Region (East Mongolia Region), which refers to Hulunbuir City, the Hinggan League, Tongliao City, Chifeng City, and the Xilin Gol League of the eastern Inner Mongolia Autonomous Region in the Northeast Economic Zone. The main types of soil are black soil, chernozems, castanozems, and grey forest soil in Northeast China, in addition to a small amount of dark-brown and brown earth [87]. The black soil region in Northeast China accounts for about one-fifth of the country's annual grain output, and is the main supplier of corn, japonica rice, and other commercial grains to China, ranking first in both grain commodity volume and grain export volume. It is also the largest natural forest region in China. The total forest stock in the mountainous areas accounts for about 1/3 of China's, and the timber output accounted for 38.4% of the country's in 1995. The area of forest is about 500,000 km², which can lengthen the melting time of snow and ice, and the snow storage in the forest is conducive to the progress of agriculture and forestry. The forest region of Changbai Mountain, which is located in the eastern part of Jilin Province, is the most complete preservation of original ecology in the world. The forest region of Hinggan Mountain is located in the northern part of Heilongjiang Province and the northeast of Inner Mongolia. Northeast China once accounted for 98% of the country's heavy industry. In 2021, the GDP of Northeast China reached 8126 billion dollars, an increase of 6.1 percent. In recent years, due to long-term high-intensity land utilization coupled with soil erosion, which results in a decrease in organic content and the degradation of physical as well as chemical properties and ecological functions. These changes have seriously threatened our country's grain production and ecological security. Therefore, it is necessary to use remote

sensing and GIS techniques to monitor the changes in forest and agricultural ecosystems in the black soil region of Northeast China, which can minimize the impact of human activities on surface conditions.

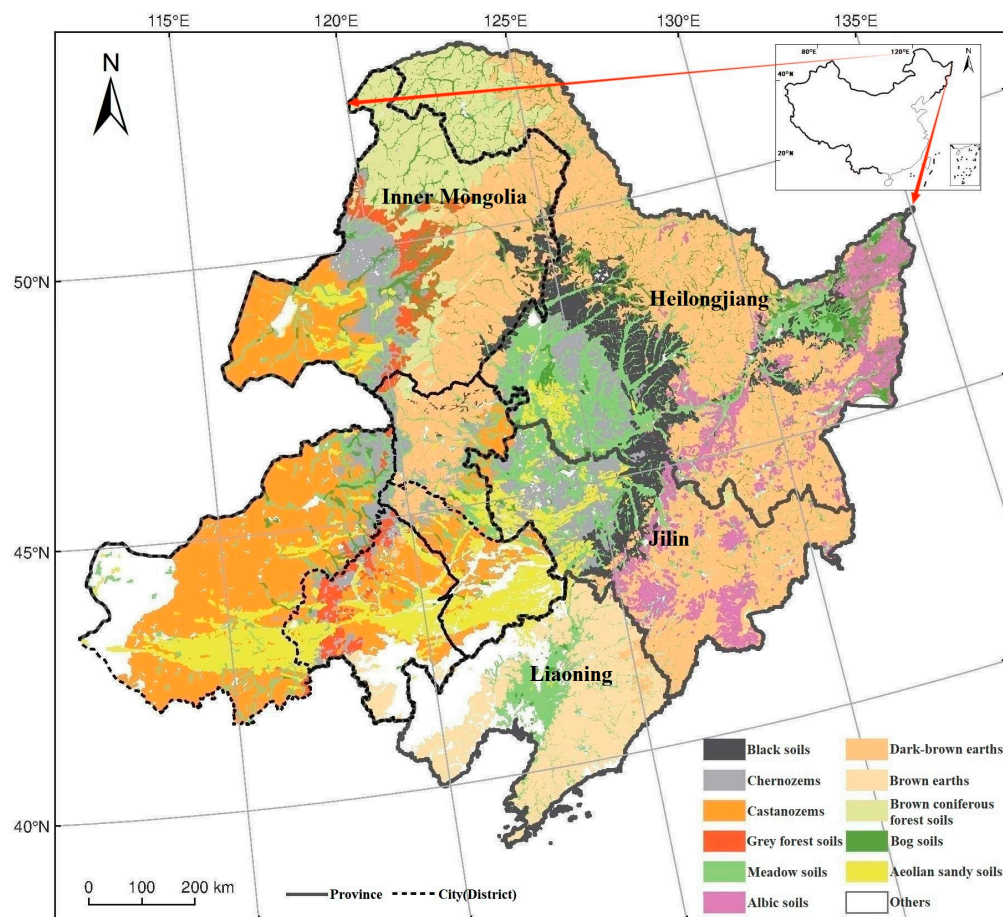


Figure 1. Distribution of the main soil types in Northeast China. Data source: a soil map (a million-scale soil map) was downloaded from the second national soil survey. The map of China and vector boundaries were from the Ministry of Natural Resources: GS(2020)3184.

2.2. Data Collection

Land cover data from 1990 to 2020 were downloaded from 30 m land cover fine classification product V1.0 at Earth System Science Data (<https://data.casearth.cn/> accessed on 18 February 2023). This product used the method of coupling change detection and dynamic updating. The main data were Landsat TM, ETM+, and OLI images, and the change detection for long time series was completed on the Google Earth Engine [88]. Combined with the change detection results, the dynamic updating of land cover was realized region-by-region and period-by-period [89,90]. We obtained 112 images covering Northeast China from 1990 to 2020, which were synthesized using Landsat images taken throughout the whole year. The fine classification system was divided into cropland (10), forest (20), grassland (30), shrubland (40), wetland (50), water bodies (60), tundra (70), impervious surfaces (80), bare areas (90), and permanent ice and snow (100) using ArcGIS 10.2 software. Among them, tundra did not exist in Northeast China, and permanent ice and snow was less than 0.25 km² from 1990 to 2020, so we ignored these two categories in the subsequent analysis. Soil data (a million-scale soil map) were downloaded from the second national soil survey (<http://vdb3.soil.csdb.cn/extend/jsp/introduction> accessed on 17 February 2023). The vector boundaries of China downloaded were a 1:1 million public version of basic geographic information data (<http://vdb3.soil.csdb.cn/extend/jsp/introduction> accessed on 17 February 2023). The map of China was downloaded from a national standard map at

the Ministry of Natural Resources: GS(2020)3184 ([http://bzdt.ch.mnr.gov.cn./download.html?SearchText=GS\(2020\)3184](http://bzdt.ch.mnr.gov.cn./download.html?SearchText=GS(2020)3184) accessed on 17 February 2023).

2.3. Methods

In this paper, we first preprocessed the original land cover data, which mainly included clipping, mosaicking, and reclassifying with ArcGIS 10.2 software. We analyzed the land cover (including black and typical black soil regions) in Northeast China from 1990 to 2020 by dynamic degree, and plotted a spatial-temporal change map of land cover. Then, the transition matrix was used to analyze the internal transition relationship of land cover from 1990 to 2000, 2000 to 2010, and 2010 to 2020. Based on the above transformation relationship and the original data, the predicted values of land cover from 1990 to 2020 were obtained by the GM (1,1) model. Finally, we analyzed the differences between the actual and predicted values, and used the GM (1,1) model to predict land cover in 2025. The methods are shown below.

2.3.1. Dynamic Degree of Land Cover

The dynamic degree of land cover can reflect the change in the quantity of land resources in addition to the change rate of different types of land cover, and can quantify the impact of human activities on land cover [91]. The single dynamic degree reflects the rate of change, and also indicates the intensity of the regional change in land cover. The higher the absolute value is, the faster the type changes. The computing formula is as follows:

$$S = \left(\frac{K_b - K_a}{K_a} \right) \times \frac{1}{n} \times 100\% \quad (1)$$

where S represents the single dynamic degree of a certain type of land cover; K_a and K_b represent the area of a certain type of land cover at the end and beginning, respectively, of the study period; and n represents the time interval.

The comprehensive dynamic degree of land cover can describe the whole change in land cover in the study area within a certain time range, reflecting the changes in regional land cover. The formula is as follows:

$$LS = \left[\frac{\sum_{i=1}^t \Delta K_{i-j}}{2 \sum_{i=1}^t K_i} \right] \times \frac{1}{n} \times 100\% \quad (2)$$

where LS represents the comprehensive degree of land cover dynamics; ΔK_{i-j} represents the absolute value of the area converted from class i to j during the initial year; K_i represents the area of class i within the study period; and n represents the time interval.

2.3.2. Transfer Matrix of Land Cover

A transfer matrix can be based on the changes in land cover at different stages to obtain a two-dimensional matrix, which was proposed by Russian mathematician Markov [92–94]. By analyzing the transition matrix of multiple time phases, we can understand the transition between different types of land cover; this is the application of the Markov model to the changes in land cover. The Markov model can not only quantitatively reflect the conversion between different types of land cover, but also reveal the transfer rate between different types of land cover. The temporal and spatial changes in different types of land cover can be obtained through the transfer matrix of land cover, and the overall status of regional ecosystem service functions caused by human activities can be understood. The brief formula of a transfer matrix is as follows:

$$P_{ab} = \begin{pmatrix} P_{11} & P_{12} & \dots & P_{1n} \\ P_{21} & P_{22} & \dots & P_{2n} \\ \dots & \dots & \dots & \dots \\ P_{n1} & P_{n2} & \dots & P_{nn} \end{pmatrix} \quad (a, b = 1, 2, 3, \dots, n) \quad (3)$$

where P_{ab} represents the area of land cover, a , converted into b before the transition; n represents the number of different types of land cover; and a and b represent the types of land cover before and after the conversion, respectively.

2.3.3. GM (1,1) Prediction Model

The GM (1,1) model was used to forecast the area of different types of land cover from 1990 to 2020, and the relationship between the actual value and the predicted value was obtained. At the same time, land cover in 2025 was forecast, and the posterior error ratio, infinitesimal error probability, root mean square error, and class ratio dispersion were calculated to verify the accuracy of the GM (1,1) model and predicted results by using Matlab 2020 and SPSS software.

The GM (1,1) model is a first-order single-variable differential equation model. It generates new data series by accumulating obvious trends in one data series. Then, the cumulative method is used for reverse calculation to recover the original data series and achieve the purpose of prediction [69,70,95]. The commonly used generation methods of the GM (1,1) model include the following: (1) cumulative sum, (2) cumulative subtraction, (3) mean generation, (4) grade ratio generation, etc. This is a kind of quantization of uncertainty by grey mathematics, which can make full use of known information to seek the inherent relationship of limited data and predict the changes in land cover in the future [71–74]; the computing formula is as follows:

- (1) Assume that the raw sequence is as follows:

$$h^{(0)} = \{h^{(0)}(1), h^{(0)}(2), \dots, h^{(0)}(i)\} \quad (4)$$

- (2) and then add up to form the following:

$$\begin{aligned} h^{(1)}(m) &= \sum_{n=1}^m h^{(0)}(n) \quad m = (1, 2, \dots, i) \\ h^{(1)} &= \{h^{(1)}(1), h^{(1)}(2), \dots, h^{(1)}(i)\} \end{aligned} \quad (5)$$

- (3) Take the average sequence:

$$y^{(1)}(m) = 0.5h^{(1)}(m) + 0.5h^{(1)}(m-1) \quad m = (2, 3, \dots, i) \quad (6)$$

- (4) The grey differential equation and albinism equation are as follows:

$$\begin{aligned} h^{(0)}(m) + ay^{(1)}(m) &= b \\ \frac{dh^{(1)}}{dt} + ah^{(1)} &= b \quad m = (2, 3, \dots, i) \end{aligned} \quad (7)$$

- (5) Introduce a matrix vector:

$$\begin{aligned} \mu &= (a, b)^T, g = \{h^{(0)}(2), \dots, h^{(0)}(i)\}^T \\ B &= \begin{bmatrix} -y^{(1)}(2) & 1 \\ -y^{(1)}(3) & 1 \\ \vdots & \vdots \\ -y^{(1)}(n) & 1 \end{bmatrix} \end{aligned} \quad (8)$$

- (6) The least squares method is used to obtain the minimum value:

$$\begin{aligned} f(\hat{\mu}) &= (g - B\hat{\mu})^T (g - B\hat{\mu}) \\ \hat{\mu} &= (a, b)^T = (B^T B)^{-1} B^T B g \end{aligned} \quad (9)$$

(7) Establishment of the prediction formula:

$$\hat{h}^{(1)}(m+1) = \left\{ \hat{h}^{(0)}(1) - \frac{b}{a} \right\} e^{-am} + \frac{b}{a} \quad (10)$$

$$\hat{h}^{(0)}(m+1) = \hat{h}^{(1)}(m+1) - \hat{h}^{(1)}(m) \quad m = (1, 2, \dots, i-1)$$

3. Results and Analysis

3.1. Spatiotemporal Change in Land Cover

After the reclassification of the original land cover data with ArcGIS software, the growth patterns of land cover in Northeast China for the years 1990, 1995, 2000, 2005, 2010, and 2020 were presented in Figure 2 and Table 1. Boundary datasets of the black and typical black soil regions were obtained from the *Digital Journal of Global Change Data Repository* [82,96]. At the same time, we plotted the change curve of forest, cropland, grassland, and bare areas, which accounted for the largest proportion of Northeast China from 1990 to 2020 (Figure 3).

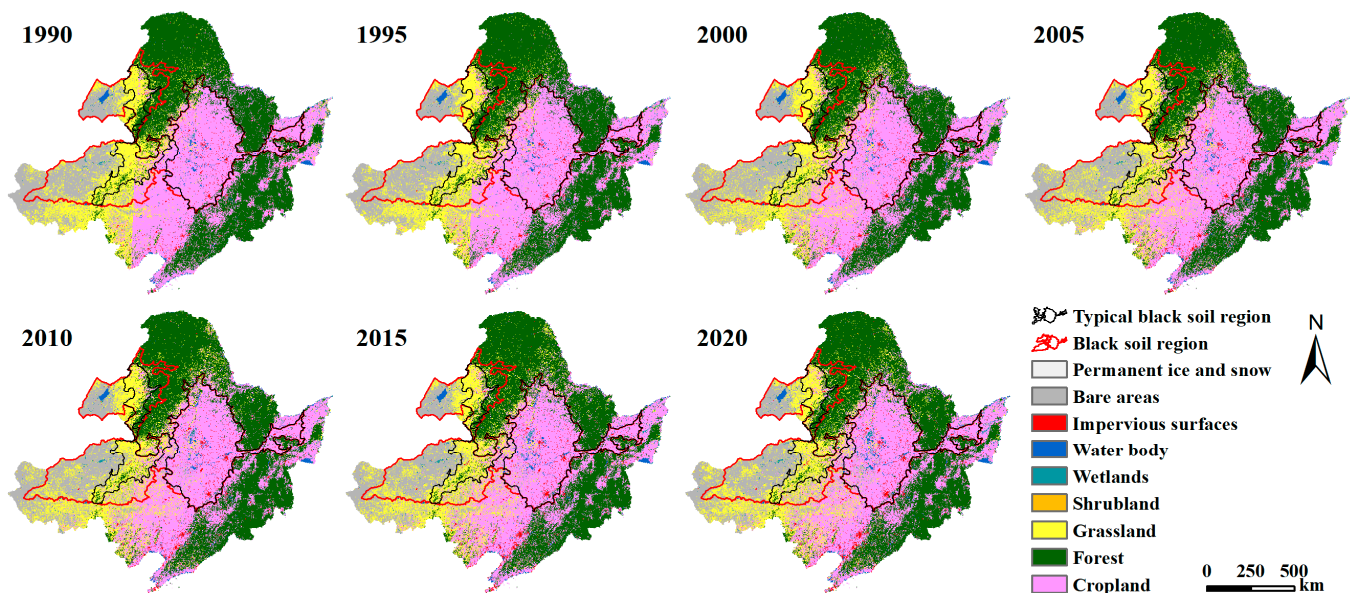


Figure 2. Land cover of Northeast China from 1990 to 2020.

Table 1. Land cover in Northeast China from 1990 to 2020 (km²).

Classification System	1990	1995	2000	2005	2010	2015	2020
Cropland	487,702	495,656	494,197	493,348	487,719	478,674	466,955
Forest	530,912	522,945	510,213	507,255	505,552	505,463	506,654
Grassland	224,906	215,457	223,364	223,379	225,166	228,165	227,482
Shrubland	42	38	430	534	632	720	1197
Wetland	4673	4906	5955	6057	6801	8814	11,121
Water bodies	15,161	15,279	15,453	16,155	16,480	17,576	17,763
Impervious surfaces	15,633	16,459	18,236	20,866	23,053	25,503	27,078
Bare areas	169,257	177,547	180,439	180,693	182,884	183,373	190,025

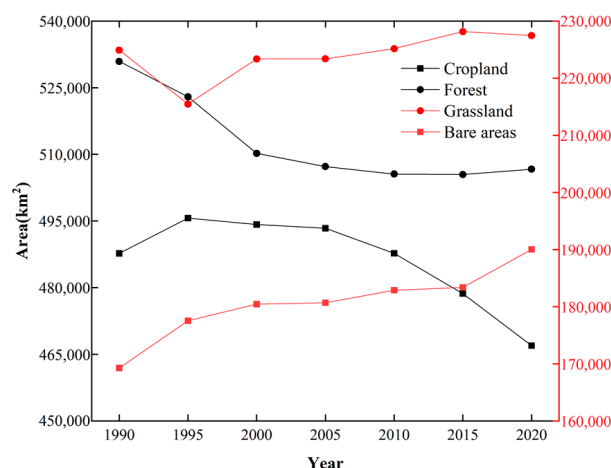


Figure 3. Change trends in cropland, forest, grassland, and bare areas from 1990 to 2020. The Y_1 axis (black) was used to describe the changes in forest and cropland areas. The Y_2 axis (red) was used to describe the changes in grassland and bare areas.

According to Figures 2 and 3, as well as Table 1, the main land cover types in the east of Northeast China were forest and cropland, accounting for approximately 37% and 34% of the total area, respectively, and were mainly distributed in Heilongjiang, Jilin, and Liaoning Provinces. The forest has been shrinking in the past 30 years; the maximum area variation was 25,449 km², with its proportion dropping from 37% in 1990 to 35% in 2015. The area of cropland first increased by 7954 km² from 1990 to 1995, but decreased by 28,071 km² from 1995 to 2020. The dominance of forest and cropland did not change from 1990 to 2020; the average area of forest and cropland was 512,713 km² and 486,322 km², respectively. Grassland and bare areas were mainly distributed in Inner Mongolia Province, accounting for 16% and 13%, respectively. The variation in the grassland area was small, at just 12,708 km², and the bare areas increased by 20,768 km² from 1990 to 2020. This geographical distribution is consistent with different land use patterns defined by human activities in Northeast China. Meanwhile, the areas of shrubland, wetland, water bodies, and impervious surfaces have been increasing. Among them, the impervious surface changed the most, increasing by 11,445 km².

A single land cover dynamic degree can not only reflect the change rate of each land type but also indicate the intensity of regional land cover change. A positive value represents the increase in land cover resources, while a negative value represents a decrease in land cover resources. A comprehensive land cover dynamic degree can also reflect the overall intensity of land cover change in two adjacent years. Except for the last row, the other rows represent a single land cover dynamic degree. The results are shown in Table 2.

Table 2. Land cover dynamics in Northeast China from 1990 to 2020.

Classification System	1990–1995	1995–2000	2000–2005	2005–2010	2010–2015	2015–2020
Cropland	0.33%	−0.06%	−0.03%	−0.23%	−0.37%	−0.49%
Forest	−0.30%	−0.49%	−0.12%	−0.07%	0.00%	0.05%
Grassland	−0.84%	0.73%	0.00%	0.16%	0.27%	−0.06%
Shrubland	−1.90%	206.32%	4.84%	3.67%	2.78%	13.25%
Wetland	1.00%	4.28%	0.34%	2.46%	5.92%	5.23%
Water bodies	0.16%	0.23%	0.91%	0.40%	1.33%	0.21%
Impervious surfaces	1.06%	2.16%	2.88%	2.10%	2.13%	1.24%
Bare areas	0.98%	0.33%	0.03%	0.24%	0.05%	0.73%
Comprehensive dynamic degree	0.24%	0.20%	0.05%	0.10%	0.13%	0.17%

According to Table 2, the land cover dynamic degree of cropland was negative, decreasing by 1.18% from 1995 to 2020, indicating that the corresponding area was decreasing continuously in this period. The intensity of cropland reduction also increased with the advancing of time, and the single dynamic degree was as high as 0.49% in 2020. This phenomenon may be related to the accelerated urbanization process in Northeast China in recent years. The forest dynamic degree decreased by 0.98% from 1990 to 2010, stabilized from 2010 to 2015, and increased by 0.05% from 2015 to 2020, indicating that the intensity of forest resource change first increased and then decreased, and that the forest in Northeast China had a certain improvement trend after 2010. The single dynamic degree of other land cover was mostly positive, indicating that the corresponding land cover resources are constantly increasing. As a whole, the change intensity from 1990 to 2000 was the highest, with a comprehensive dynamic degree greater than 0.20%. Since 2000, the comprehensive dynamic degree decreased to 0.05% and then increased to 0.17%. The results showed that the intensity of land cover change first decreased and then increased, which may be related to the drastic fluctuation in cropland area caused by human activities in the black soil region.

We also calculated the changes in different types of land cover in the black and typical black soil regions, as shown in Tables 3 and 4. By analyzing the change in land cover in these two regions, soil and water erosion in the black soil region of Northeast China can be understood to a certain extent.

Table 3. Change in land cover in the black soil region from 1990 to 2020 (km²).

Classification System	1990	1995	2000	2005	2010	2015	2020
Cropland	238,282	239,426	238,862	236,084	232,975	228,328	224,562
Forest	59,656	58,207	55,592	55,904	56,070	55,851	56,372
Grassland	129,156	122,578	121,341	122,123	122,199	124,138	120,561
Shrubland	23	13	71	106	111	106	167
Wetland	2389	2417	2802	2924	3395	4292	5400
Water bodies	7487	7490	7332	8002	8191	9107	9224
Impervious surfaces	7440	7763	8459	9530	10,307	11,228	11,847
Bare areas	112,091	118,630	122,065	121,851	123,276	123,474	128,388

Table 4. Change in land cover in the typical black soil region from 1990 to 2020 (km²).

Classification System	1990	1995	2000	2005	2010	2015	2020
Cropland	214,825	216,152	215,876	214,572	212,044	207,788	204,600
Forest	34,118	33,046	30,397	30,347	30,415	31,515	31,593
Grassland	68,128	66,179	65,333	62,655	62,764	64,050	62,596
Shrubland	17	10	30	49	27	14	33
Wetland	859	793	1213	1376	1479	2326	3415
Water bodies	4803	4704	4597	5399	5773	6377	6446
Impervious surfaces	7023	7306	7909	8872	9548	10,336	10,869
Bare areas	3249	4832	7667	9752	10,972	10,617	13,467

According to Tables 3 and 4, the area of cropland, forest, and grassland has been decreasing, and the area of shrubland, wetland, water bodies, impervious surfaces, and bare areas has been increasing. The average area of forest over the last thirty years was only 56,807 km² and 31,633 km² in the black and typical black soil regions, respectively, and cropland covered 234,074 km² and 212,265 km², respectively. Cropland was dominant and forest was less so, but the area of cropland in both regions decreased by 14,864 km² and 11,552 km² from 1990 to 2020, respectively. At the same time, the area of bare areas increased by 16,297 km² and 10,218 km², respectively. The phenomenon may also be related to urbanization and land loss. In addition, the average area of grassland and bare areas in

the black soil region was 58,628 km² and 112,745 km² more than that in the typical black soil region, respectively. This phenomenon is also related to the different patterns of land use (mainly grassland grazing) in Inner Mongolia, which can be seen in Figure 2.

3.2. Transfer Matrix of Land Cover

A raster calculator was used to extract the transfer matrix of land cover from 1990 to 2000, 2000 to 2010, and 2010 to 2020. Here, we calculated the land cover transfer matrix on a ten-year basis. We can obtain the temporal and spatial changes in different types of land cover and understand the overall status of regional ecosystem service functions from land cover change (Tables 5 and 6). In Table 6, the upper and lower rows represent the transfer matrix of land cover from 2000 to 2010 and 2010 to 2020, respectively.

Table 5. Transfer matrix of land cover from 1990 to 2000 (km²).

Land Cover ID	2000								
	10	20	30	40	50	60	80	90	
1990	10	436,540	14,167	25,217	44	2081	2028	2230	5395
	20	27,682	484,057	18,346	24	436	269	60	37
	30	23,764	11,645	148,680	111	482	172	188	39,864
	40	7	0	8	5	0	1	0	20
	50	1360	211	342	0	2101	242	7	410
	60	1801	121	116	1	313	12,683	34	91
	80	0	0	0	0	0	0	15,633	0
	90	3043	12	30,654	245	541	58	83	134,621

Classification system and its land cover ID: cropland (10), forest (20), grassland (30), shrubland (40), wetland (50), water bodies (60), tundra (70), impervious surfaces (80), and bare areas (90).

Table 6. Transfer matrix of land cover from 2000 to 2010 and 2010 to 2020 (km²).

Land Cover ID	2010–2020								
	10	20	30	40	50	60	80	90	
10	444,480	11,808	23,189	21	2128	2566	4146	5860	
	430,329	11,842	24,440	100	4869	2146	3277	10,704	
20	13,473	480,771	15,236	56	292	282	76	28	
	9795	480,478	14,424	279	199	208	111	58	
30	22,495	12,467	161,856	63	495	292	299	25,397	
	19,775	13,840	168,679	70	690	117	298	21,695	
40	23	8	11	359	0	0	0	28	
	11	28	8	547	5	1	1	32	
50	1735	358	389	3	2659	332	23	457	
	1304	326	244	4	3898	611	44	369	
60	1354	106	90	3	580	12,960	134	227	
	994	110	31	2	656	14,543	114	30	
80	9	0	1	0	0	0	18,225	0	
	9	0	1	0	2	0	23,041	0	
90	4149	33	24,395	127	647	49	151	150,888	
	4738	29	19,656	194	800	137	192	157,136	

According to Tables 5 and 6, the average area of cropland, forest, grassland, and bare areas from 1990 to 2000, 2000 to 2010, and 2010 to 2020 that remained unchanged was 437,116 km², 481,768 km², 159,738 km², and 147,548 km². The area of cropland converted into forest and grassland was 14,167 km² and 25,217 km², respectively, and the area of forest and grassland converted into cropland was 27,682 km² and 23,764 km², respectively (Table 5). Meanwhile, the area conversion of forest and grassland was 18,346 km² and

11,645 km², respectively. It can be seen that cropland, forest, and grassland were converted into each other. Moreover, grassland and bare areas were also converted into each other; the area conversion of them was 39,864 km² and 30,654 km².

Table 6 also shows the same conversion rules of land cover. Between 2000 and 2010, the area of cropland converted into forest and grassland was 11,808 km² and 23,189 km², respectively. The area of forest converted into cropland and grassland was 13,473 km² and 15,236 km², respectively, and the area of grassland converted into cropland and forest was 22,495 km² and 12,467 km², respectively. The area conversion of grassland and bare areas was 25,397 km² and 24,395 km², respectively. Between 2010 and 2020, the conversion area between cropland and forest was 11,842 km² and 9795 km², respectively, and the conversion area between cropland and grassland was 24,440 km² and 19,775 km², respectively. The area of forest and grassland converted into each other is 14,424 km² and 13,840 km², respectively. Meanwhile, the area conversion of grassland and bare areas was 21,695 km² and 19,656 km², respectively. It should be noted that the area converted from cropland into bare areas was as high as 10,704 km² from 2010 to 2020. Such a large transformation from cropland into bare areas has not happened before. To sum up, the mutual conversion between cropland, forest, grassland, and bare areas was the most frequent from 1990 to 2020. We can better understand the curve changes in different land covers in Figure 3 through such rules and develop strategies as well as means to minimize the impact of human activities on land cover.

3.3. Prediction of Land Cover

The GM (1,1) model was used to predict the area of different types of land cover from 1990 to 2025 (Table 7), and the original data used in the prediction process are shown in Table 1. We can clearly understand the differences between the predicted and actual values in Tables 1 and 7 and can also obtain the change in land cover by 2025 from historical data.

Table 7. The predicted results of land cover from 1990 to 2025 (km²).

Land Cover ID	10	20	30	40	50	60	80	90
1990	487,702	530,912	224,906	42	4673	15,161	15,633	169,257
1995	500,079	516,704	218,447	128	4431	15,111	16,781	177,269
2000	494,397	513,874	220,574	297	5466	15,622	18,543	179,326
2005	488,780	511,058	222,722	478	6571	16,151	20,491	181,406
2010	483,226	508,258	224,890	670	7749	16,698	22,642	183,511
2015	477,736	505,474	227,080	876	9005	17,264	25,019	185,640
2020	472,308	502,705	229,291	1095	10,345	17,848	27,647	187,794
2025	466,942	499,950	231,524	1329	11,775	18,453	30,549	189,973

According to Tables 1 and 7, the maximum residuals between the predicted and actual values of cropland, forest, grassland, shrubland, wetland, water bodies, impervious surfaces, and bare areas were −5353 km², 6241 km², −2990 km², −156 km², −948 km², 312 km², −569 km², and −2267 km², respectively, from 1990 to 2020. Meanwhile, except for shrubland, the maximum relative errors of the other types of land cover were the same as the years of the maximum residuals. The maximum relative errors of cropland, forest, grassland, water bodies, impervious surfaces, and bare areas were controlled within 2%. The reason for this phenomenon was that the area of shrubland suddenly increased from 38 km² to 430 km² between 1995 and 2000 in Table 1. The area of shrubland was also the smallest in 1995, and a higher compensation value was introduced into the predicted value to meet the fitting requirements of the GM (1,1) model. Therefore, the maximum relative error between the predicted and actual values of shrubland appeared in 1995 rather than 2015. The predicted values of cropland, forest, grassland, shrubland, wetland, water bodies, impervious surfaces, and bare areas were 466,942 km², 499,950 km², 231,524 km², 1329 km², 11,775 km², 18,453 km², 30,549 km², and 189,973 km² by 2025 (Table 7).

In addition, the posteriori error ratio, root mean square error, infinitesimal error probability, and class ratio dispersion were computed to verify the accuracy of the GM (1,1) model, as shown in Table 8.

Table 8. Prediction accuracy of the GM (1,1) model.

Land Cover ID	10	20	30	40	50	60	80	90
Posteriori error ratio	0.142	0.147	0.206	0.066	0.071	0.031	0.009	0.052
Class ratio dispersion	0.009	0.006	0.016	0.249	0.081	0.018	0.018	0.012
Root mean square error (km ²)	3877	3867	1901	104	614	187	421	1434
Infinitesimal error probability	1	1	0.714	1	1	1	1	1
Ratings	Good	Good	Good	Eligible	Good	Good	Good	Good

As can be seen from Table 8, all of the ratings predicted by the GM (1,1) model were good except for those for shrubland, which was eligible. Generally, if the posteriori error ratio and class ratio dispersion are less than 0.35 and 0.2, respectively, the accuracy level of the GM (1,1) model is good. If the infinitesimal error probability is between 0.7 and 1, the accuracy level is qualified. It can be found that basically all of the indicators were within the range of the requirements. The root mean square error of cropland, forest, grassland, shrubland, wetland, water bodies, impervious surfaces, and bare areas were 3877 km², 3867 km², 1901 km², 104 km², 614 km², 187 km², 421 km², and 1434 km², which was acceptable in the case of a large area. The forecast results can also provide some reference for policymakers and managers in the comprehensive management of regional surface conditions.

4. Discussion

Dynamic monitoring and spatiotemporal analyses of land cover have always been key issues in the study of the impact of human activities on ecological environmental protection [97–99]. Firstly, the spatiotemporal changes in land cover in the black soil region of Northeast China in the last thirty years were obtained by using remote sensing and GIS techniques [100–102]. The dynamic degree of land cover was used to quantify the impact of human activities on land cover. Secondly, a transfer matrix was used to reveal the dynamic conversion of land cover from 1990 to 2000, 2000 to 2010, and 2010 to 2020, and the GM (1,1) model was used to forecast the change in land cover by 2025 based on historical data. Finally, we evaluated the accuracy of the predicted values and the GM (1,1) model.

In this article, Northeast China included Heilongjiang, Jilin, Liaoning, and parts of Inner Mongolia Province (Figure 1), which was consistent with the vector boundary used by Liu [87]; however, many scholars ignored the five League cities in eastern Inner Mongolia when they analyzed the changes in land cover in Northeast China, which led to differences in analyzing land cover [82]. Our study area is one of only three large black soil regions in the world, and the forest is mainly distributed in the Greater Khingan Mountains, the Lesser Khingan Mountains, and the Changbai Mountains. The cropland is mainly distributed in the Sanjiang, Songnen, and Mengdong black soil region. Despite the fertile soil, large-scale agricultural development largely took place from 1900 [79]; therefore, the analysis of land cover in Northeast China started from 1990 in this paper. The results suggested that forest area has been decreasing in the past 30 years; the maximum area variation was 25,449 km², with its proportion dropping from 37% in 1990 to 35% in 2015 (Table 1). Zhao et al. found that the forest area decreased significantly from 1989 to 2006 [75], which was consistent with the results we obtained. It can be found that the change curve of forest area also declined significantly from 1990 to 2005 and became stable from 2005 (Figure 3). Deng et al. found that the forest area decreased by 21,100 km² in Northeast China from 1988 to 2005 (4.99×10^5 km² in 2005) [80], and our results showed a loss of 23,687 km² of forest area (5.07×10^5 km² in 2005) (Table 1). To some extent, the results were very similar when ignoring the range of different study areas. At the same time, Zhao et al. found

that the expansion of cropland was the major change during 1986–2000 [75], which was consistent with the change trend in cropland that we obtain from 1990 to 2000 (Figure 3). Considering the accuracy evaluation of land cover maps from 1990 to 2020, it was necessary to discuss the quality of the data used in this paper. The overall accuracy of the local adaptive random forest classification model in 2015 under the first-class system (forest, cropland, permanent ice and snow, bare areas, water bodies, impervious surfaces, grassland, shrubland, wetland, and tundra) was 81.4%, and the kappa coefficient was 0.77. The above land cover classification was also the ranking of classification accuracy; the classification accuracy of the ground class, with relatively simple spectral characteristics and a greater area proportion, was higher. However, under the LCCS classification system (sixteen land cover classifications), the overall accuracy was 71.4% and the kappa coefficient was 0.686. An overall accuracy of 68.7% and a kappa coefficient of 0.662 were achieved for the LCCS level-2 system (twenty-four land cover classifications). The reason for this phenomenon was that the LCCS system contained more similar land classes, forest was divided into evergreen broad-leaved forest, deciduous broad-leaved forest, evergreen coniferous forest, deciduous coniferous forest, and mixed forest, and there was often more serious confusion among similar land classes [89,90]. The dynamic monitoring and analysis of land cover in this paper can also provide some references for surface change in the black soil region of China [103,104].

From the perspective of research methods, we used the dynamic degree of land cover, spatial analysis, a transfer matrix, and the GM (1,1) model. Among them, the dynamic degree can reflect the rate of land cover change and also indicate the intensity of the regional change in land cover. Spatial analysis is the quantitative study of geospatial phenomena, and it is the core of remote sensing and GIS. By using spatial analysis, we can describe the evolutionary process and spatiotemporal association of land cover adequately [105,106]. Meanwhile, the transfer matrix can define the important processes of changes in land cover [107]; we can obtain the temporal and spatial changes in different land cover types and understand the overall status of regional ecosystem service functions from land cover change. In addition, the use of long time series data also provides opportunities for the prediction of land cover in the future, such as the dynamics of land system (DLS) model [65], land change evaluation model [66], CA-Markov model [68,108,109], and GM (1,1) model [70]. Deng et al. simulated the spatial changes in forest area in northeast China from 2000 to 2020 using the DLS model based on an analysis of the period between 1988 and 2000 [65]. Devi et al. forecasted the scenarios of land cover between 2045, 2073, and 2100 using land change evaluation (MOLUSCE) modules in QGIS [66]. Nath et al. predicted land cover in 2025, 2030, and 2040 by using the CA-Markov model based on 2007 and 2018 data [41]. Li et al. used the LCM model to predict the land cover in 2030 based on historical data from 1980 to 2018 [110]. Singh et al. also used a land change modeler (LCM) module to obtain future urban growth in 2030 based on datasets from 2010 and 2020 [111]; however, the above methods also had some limitations. The DLS model required multiple simulations to determine the optimal model parameters. The land change evaluation model and CA-Markov model were not suitable for medium- and long-term forecasting. Most of the work produced maps of land cover in sparser time series; there were only a few historical data used for modeling and predicting the future. Therefore, GM (1,1) was widely used because it took into account all historical data when the original sequence data were limited. The prediction GM (1,1) model is a first-order single-variable differential equation model. It generates new data series by accumulating obvious trends in one data series. The cumulative method is then used for reverse calculation to recover the original data series and achieve the purpose of prediction [112,113]. This approach also has its limitations: more accurate results can be obtained when the annual land cover area change is not a sudden and small leap, or presents an exponential change. The results are best when only the latter phase of land cover is predicted, and the continuous prediction of multiple stages will result in a large deviation in the results. As described in Section 3.3, the maximum relative error of shrubland between the prediction results and actual values is the largest,

and the corresponding model is evaluated as eligible, which is the worst result of all. The reason is that the area of shrubland was the smallest in 1995, and more compensation values were introduced into the predicted values to meet the fitting requirements of the GM (1,1) model.

Most scholars focused on the soil and environment in Northeast China [114–116], and there were few studies on the change in land cover in recent years, which limited the analysis of the changes in agricultural and forestry ecosystems caused by human activities in Northeast China. This study can better analyze the spatiotemporal changes in land cover and understand the internal conversion law of forest, farmland, grassland, and other types of land cover in the past 30 years, and can also provide some experience for further analyzing the spatial and temporal changes in land cover and its future prediction in Northeast China. There are many methods to predict land cover, but each method has its limitations in some aspects. How to combine deep learning and the CA-Markov as well as GM (1,1) models to forecast and analyze the change in land cover is also a challenge. In addition, it is essential to choose suitable comparative analysis regions and more advanced means to further quantitatively analyze the effect of spectral as well as biophysical/biochemical parameters, land disturbance, and climate change on land cover; this will be the focus of subsequent research.

5. Conclusions

Based on remote sensing and GIS techniques, this paper analyzed and quantified the spatial and temporal changes in land cover caused by human activities and policies in Northeast China in the past three decades, and predicted the change in land cover in 2025.

The forest area has been decreasing in the past 30 years; the maximum area variation was 25,449 km², with its proportion dropping from 37% in 1990 to 35% in 2015. The area of cropland first increased by 7954 km² from 1990 to 1995, but decreased by 28,071 km² from 1995 to 2020. The dominance of forest and cropland did not change from 1990 to 2020; the average area of forest and cropland was 512,713 km² and 486,322 km², respectively. Grassland and bare areas were mainly distributed in Inner Mongolia Province, accounting for 16% and 13%, respectively. The variation in the grassland area was small, at just 12,708 km², and the bare areas increased by 20,768 km² from 1990 to 2020. Via comparison with other studies, the temporal and spatial changes in land cover can not only help to understand the surface conditions of different regions but also provide a basis for comprehensive management in Northeast China.

The mutual conversion between cropland, forest, grassland, and bare areas was the most frequent. The area of cropland converted into forest and grassland was 14,167 km² and 25,217 km², respectively, and the area of forest and grassland converted into cropland was 27,682 km² and 23,764 km², respectively, from 1990 to 2000. Meanwhile, the area conversion of forest and grassland was 18,346 km² and 11,645 km², respectively. Moreover, grassland and bare areas were also converted into each other; the area conversion of them was 39,864 km² and 30,654 km², respectively. A similar law of land cover change was also presented from 2000 to 2020. It should be noted that the area converted from cropland into bare areas was as high as 10,704 km² from 2010 to 2020. The phenomenon may be related to urbanization and land loss.

The maximum residuals between the predicted and actual values of cropland, forest, grassland, shrubland, wetland, water bodies, impervious surfaces, and bare areas were −5353 km², 6241 km², −2990 km², −156 km², −948 km², 312 km², −569 km², and −2267 km² from 1990 to 2020. The predicted values of cropland, forest, grassland, shrubland, wetland, water bodies, impervious surfaces, and bare areas were 466,942 km², 499,950 km², 231,524 km², 1329 km², 11,775 km², 18,453 km², 30,549 km², and 189,973 km² in 2025. It was found that the predicted values (the maximum residual) and all of the evaluation indices were within the acceptable range, and using as many years of land cover data as possible to predict the next year can minimize abrupt changes in land cover. This

study can also provide some experience for further analyzing the spatial and temporal changes in land cover and its future prediction in Northeast China.

Author Contributions: Conceptualization, Ding Ma and Liang Xu; writing—review and editing, Ding Ma; data curation, Ding Ma; formal analysis, Ding Ma; investigation, Ding Ma; writing—original draft, Ding Ma; methodology, Ding Ma; resources, Xin Tan; software, Ding Ma; supervision, Ding Ma; validation, Ding Ma, Sijia Jiang, Mingyu Yang and Qingbin Jiao; visualization, Ding Ma, Liang Xu and Mingyu Yang. All authors have read and agreed to the published version of the manuscript.

Funding: This research was funded by the Scientific and Technological Innovation Project of Black Land Protection and Utilization (XDA28050201); Jilin Province Database of Agriculture Spectrum Application Information (20230505009ZP); National Natural Science Foundation of China (NSFC) (61975199); Capital construction funds in Jilin Province in 2023 (2023C036-4); Changchun science and technology development plan project (22SH03); Jilin Province Science and Technology Development Plan Project (20220201060GX); Jilin province and Chinese Academy of Sciences Science and Technology Cooperation High Tech Special Fund project (2023SYHZ0020).

Data Availability Statement: Soil data (a million-scale soil map) were downloaded from the second national soil survey (<http://vdb3.soil.csdb.cn/extend/jsp/introduction> accessed on 17 February 2023). Land cover data were downloaded from 30 m land cover fine classification product V1.0 at Earth System Science Data (<https://data.casearth.cn/> accessed on 18 February 2023). The vector boundaries of China were obtained from basic geographic information data (<https://www.webmap.cn/commres.do?method=result100W> accessed on 17 February 2023). The map of China was downloaded from the Ministry of Natural Resources: GS(2020)3184 ([http://bzdt.ch.mnr.gov.cn/download.html?SearchText=GS\(2020\)3184](http://bzdt.ch.mnr.gov.cn/download.html?SearchText=GS(2020)3184) accessed on 17 February 2023).

Conflicts of Interest: The authors declare no conflict of interest.

References

1. Marchant, R.; Richer, S.; Boles, O.; Capitani, C.; Courtney-Mustaphi, C.J.; Lane, P.; Prendergast, M.E.; Stump, D.; Cort, G.D.; Kaplan, J.O.; et al. Drivers and trajectories of land cover change in East Africa: Human and environmental interactions from 6000 years ago to present. *Earth-Sci. Rev.* **2018**, *178*, 322–378. [[CrossRef](#)]
2. Martins, I.S.; Dornelas, M.; Vellend, M.; Thomas, C.D. A millennium of increasing diversity of ecosystems until the mid-20th century. *Glob. Change Biol.* **2022**, *28*, 5945–5955. [[CrossRef](#)] [[PubMed](#)]
3. Brown, J.F.; Tollerud, H.J.; Barber, C.P.; Zhou, Q.; Dwyer, J.L.; Vogelmann, J.E.; Loveland, T.R.; Woodcock, C.E.; Stehman, S.V.; Zhu, Z.; et al. Lessons learned implementing an operational continuous United States national land change monitoring capability: The land change monitoring, assessment, and projection (LCMAP) approach. *Remote Sens. Environ.* **2020**, *238*, 111356. [[CrossRef](#)]
4. Morshed, S.R.; Fattah, M.A.; Haque, M.N.; Morshed, S.Y. Future ecosystem service value modeling with land cover dynamics by using machine learning based Artificial Neural Network model for Jashore city, Bangladesh. *Phys. Chem. Earth* **2022**, *126*, 103021. [[CrossRef](#)]
5. Gong, Y.; Cai, M.; Yao, L.; Cheng, L.; Hao, C.; Zhao, Z. Assessing changes in the ecosystem services value in response to land-use/land-cover dynamics in Shanghai from 2000 to 2020. *Int. J. Environ. Res. Public Health* **2022**, *19*, 12080. [[CrossRef](#)]
6. Ellis, E.C.; Beusen, A.H.W.; Goldewijk, K.K. Anthropogenic biomes: 10,000 BCE to 2015 CE. *Land* **2020**, *9*, 129. [[CrossRef](#)]
7. Olorunfemi, I.E.; Fasinmirin, J.T.; Olufayo, A.A.; Komolafe, A.A. GIS and remote sensing-based analysis of the impacts of land use/land cover change (LULCC) on the environmental sustainability of Ekiti State, southwestern Nigeria. *Environ. Dev. Sustain.* **2020**, *22*, 661–692. [[CrossRef](#)]
8. Hailu, A.; Mammo, S.; Kidane, M. Dynamics of land use, land cover change trend and its drivers in Jimma Geneti District, Western Ethiopia. *Land Use Policy* **2020**, *99*, 105011. [[CrossRef](#)]
9. Roy, P.S.; Ramachandran, R.M.; Paul, O.; Thakur, P.K.; Ravan, S.; Behera, M.D.; Kanawade, V.P. Anthropogenic land use and land cover changes—A review on its environmental consequences and climate change. *J. Indian Soc. Remote.* **2022**, *50*, 1615–1640. [[CrossRef](#)]
10. Esfandeh, S.; Danehkar, A.; Salmanmahiny, A.; Sadeghi, S.M.M.; Marcu, M.V. Climate change risk of urban growth and land use/land cover conversion: An in-depth review of the recent research in Iran. *Sustainability* **2022**, *14*, 338. [[CrossRef](#)]
11. Hussain, S.; Lu, L.; Mubeen, M.; Nasim, W.; Karuppanan, S.; Fahad, S.; Tariq, A.; Mousa, B.G.; Mumtaz, F.; Aslam, M. Spatiotemporal variation in land use land cover in the response to local climate change using multispectral remote sensing data. *Land* **2022**, *11*, 595. [[CrossRef](#)]
12. Hurtt, G.C.; Chini, L.; Sahajpal, R.; Frohling, S.; Bodirsky, B.L.; Calvin, K.; Doelman, J.C.; Fisk, J.; Fujimori, S.; Goldewijk, K.K.; et al. Harmonization of global land use change and management for the period 850–2100 (LUH2) for CMIP6. *Geosci. Model Dev.* **2020**, *13*, 5425–5464. [[CrossRef](#)]

13. Zhu, Z.; Qiu, S.; Ye, S. Remote sensing of land change: A multifaceted perspective. *Remote Sens. Environ.* **2022**, *282*, 113266. [[CrossRef](#)]
14. Olorunfemi, I.E.; Olufayo, A.A.; Fasinmirin, J.T.; Komolafe, A.A. Dynamics of land use land cover and its impact on carbon stocks in Sub-Saharan Africa: An overview. *Environ. Dev. Sustain.* **2022**, *24*, 40–76. [[CrossRef](#)]
15. Msofe, N.K.; Sheng, L.; Li, Z.; Lyimo, J. Impact of land use/cover change on ecosystem service values in the Kilombero valley floodplain, Southeastern Tanzania. *Forests* **2020**, *11*, 109. [[CrossRef](#)]
16. Juknelienė, D.; Česonienė, L.; Jonikavičius, D.; Šileikienė, D.; Tiškutė-Memgaidienė, D.; Valčiukienė, J.; Mozgeris, G. Development of land cover naturalness in Lithuania on the edge of the 21st Century: Trends and driving factors. *Land* **2022**, *11*, 339. [[CrossRef](#)]
17. Sourn, T.; Pok, S.; Chou, P.; Nut, N.; Theng, D.; Rath, P.; Reyes, M.R.; Prasad, P.V.V. Evaluation of land use and land cover change and its drivers in Battambang Province, Cambodia from 1998 to 2018. *Sustainability* **2021**, *13*, 11170. [[CrossRef](#)]
18. Velastegui-Montoya, A.; Montalván-Burbano, N.; Peña-Villacreses, G.; de Lima, A.; Herrera-Franco, G. Land use and land cover in tropical forest: Global research. *Forests* **2022**, *13*, 1709. [[CrossRef](#)]
19. Pulighe, G. Perspectives and advancements on “land use and land cover mapping in a changing world”. *Land* **2022**, *11*, 2108. [[CrossRef](#)]
20. Cianciullo, S.; Attorre, F.; Trezza, F.R.; Rezende, M.; Ntumi, C.; Campira, J.; Munjovo, T.E.; Timane, D.R.; Riccardi, T.; Malatesta, L. Analysis of land cover dynamics in Mozambique (2001–2016). *Rend. Lincei-Sci. Fis.* **2023**, *34*, 81–92. [[CrossRef](#)]
21. Shi, F.; Yang, B.; Li, M. An improved framework for assessing the impact of different urban development strategies on land cover and ecological quality changes-A case study from Nanjing Jiangbei New Area, China. *Ecol. Indic.* **2023**, *147*, 109998. [[CrossRef](#)]
22. Xie, Q.; Han, Y.; Zhang, L.; Han, Z. Dynamic evolution of land use/land cover and its socioeconomic driving forces in Wuhan, China. *Int. J. Environ. Res. Public Health* **2023**, *20*, 3316. [[CrossRef](#)]
23. Li, Z.; Lu, Y.; Yang, X. Multi-level dynamic analysis of landscape patterns of Chinese megacities during the period of 2016–2021 based on a spatiotemporal land-cover classification model using high-resolution satellite imagery: A case study of Beijing, China. *Remote Sens.* **2023**, *15*, 74. [[CrossRef](#)]
24. Pan, W.; Wang, S.; Wang, Y.; Yu, Y.; Luo, Y. Dynamical changes of land use/land cover and their impacts on ecological quality during China’s reform periods: A case study of Quanzhou city, China. *PLoS ONE* **2022**, *17*, e0278667. [[CrossRef](#)]
25. Xie, S.; Liu, L.; Zhang, X.; Yang, J. Mapping the annual dynamics of land cover in Beijing from 2001 to 2020 using Landsat dense time series stack. *ISPRS J. Photogramm. Remote Sens.* **2022**, *185*, 201–218. [[CrossRef](#)]
26. Zhai, H.; Lv, C.; Liu, W.; Yang, C.; Fan, D.; Wang, Z.; Guan, Q. Understanding spatio-temporal patterns of land use/land cover change under urbanization in Wuhan, China, 2000–2019. *Remote Sens.* **2021**, *13*, 3331. [[CrossRef](#)]
27. Chen, W.; Chi, G.; Li, J. Ecosystem services and their driving forces in the middle reaches of the Yangtze river urban agglomerations, China. *Int. J. Environ. Res. Public Health* **2020**, *17*, 3717. [[CrossRef](#)] [[PubMed](#)]
28. Peng, D.; Zhen, H. Quantifying land use/land cover change and urban expansion in Dongguan, China, from 1987 to 2020. *IEEE J. Sel. Top Appl. Earth Obs. Remote Sens.* **2022**, *15*, 201–209. [[CrossRef](#)]
29. Alawamy, J.S.; Balasundram, S.K.; Mohd. Hanif, A.H.; Boon Sung, C.T. Detecting and analyzing land use and land cover changes in the region of Al-Jabal Al-Akhdar, Libya using time-series Landsat data from 1985 to 2017. *Sustainability* **2020**, *12*, 4490. [[CrossRef](#)]
30. Sarif, M.O.; Gupta, R.D. Spatiotemporal mapping of Land Use/Land Cover dynamics using Remote Sensing and GIS approach: A case study of Prayagraj City, India (1988–2018). *Environ. Dev. Sustain.* **2022**, *24*, 888–920. [[CrossRef](#)]
31. Aka, K.S.R.; N’da Dibi, H.; Koffi, J.N.D.; Bohoussou, C.N. Land cover dynamics and assessment of the impacts of agricultural pressures on wetlands based on earth observation data: Case of the Azagny Ramsar site in Southern Côte d’Ivoire. *J. Geosci. Environ. Prot.* **2022**, *10*, 43–61. [[CrossRef](#)]
32. Sun, T.; Cheng, W.; Abdelkareem, M.; Al-Arifi, N. Mapping prospective areas of water resources and monitoring land use/land cover changes in an arid region using remote sensing and GIS techniques. *Water* **2022**, *14*, 2435. [[CrossRef](#)]
33. Chowdhury, S.; Peddle, D.R.; Wulder, M.A.; Heckbert, S.; Shipman, T.C.; Chao, D.K. Estimation of land-use/land-cover changes associated with energy footprints and other disturbance agents in the upper peace region of Alberta Canada from 1985 to 2015 using Landsat data. *Int. J. Appl. Earth Obs. Geoinf.* **2021**, *94*, 102224. [[CrossRef](#)]
34. Kumar, S.; Singh, V.; Saroha, J. Interpretation of land use/land cover dynamics with the application of geospatial techniques in sarbari khad watershed of Himachal Pradesh, India. *GeoJournal* **2022**, *88*, 2623–2633. [[CrossRef](#)]
35. Hemati, M.; Hasanlou, M.; Mahdianpari, M.; Mohammadimanesh, F. A systematic review of Landsat data for change detection applications: 50 years of monitoring the earth. *Remote Sens.* **2021**, *13*, 2869. [[CrossRef](#)]
36. El Haj, F.A.; Ouadif, L.; Akhssas, A. Monitoring land use and land cover change using remote sensing techniques and the precipitation-vegetation indexes in Morocco. *Ecol. Eng. Environ. Technol.* **2023**, *24*, 272–286. [[CrossRef](#)]
37. Potapov, P.; Hansen, M.C.; Kommareddy, I.; Kommareddy, A.; Turubanova, S.; Pickens, A.; Adusei, B.; Tyukavina, A.; Ying, Q. Landsat analysis ready data for global land cover and land cover change mapping. *Remote Sens.* **2020**, *12*, 426. [[CrossRef](#)]
38. Liu, B.; Pan, L.; Qi, Y.; Guan, X.; Li, J. Land use and land cover change in the Yellow River Basin from 1980 to 2015 and its impact on the ecosystem services. *Land* **2021**, *10*, 1080. [[CrossRef](#)]
39. Zhao, S.; Fan, Z.; Gao, X. Spatiotemporal dynamics of land cover and their driving forces in the Yellow River Basin since 1990. *Land* **2022**, *11*, 1563. [[CrossRef](#)]

40. Comber, A.; Wulder, M. Considering spatiotemporal processes in big data analysis: Insights from remote sensing of land cover and land use. *Trans. GIS* **2019**, *23*, 879–891. [[CrossRef](#)]
41. Nath, B.; Wang, Z.; Ge, Y.; Islam, K.P.; Singh, R.; Niu, Z. Land use and land cover change modeling and future potential landscape risk assessment using Markov-CA model and analytical hierarchy process. *ISPRS Int. J. Geo-Inf.* **2020**, *9*, 134. [[CrossRef](#)]
42. Cieślak, I.; Biłozor, A.; Żróbek-Sokolnik, A.; Zagroba, M. The use of geographic databases for analyzing changes in land cover—A case study of the region of Warmia and Mazury in Poland. *ISPRS Int. J. Geo-Inf.* **2020**, *9*, 358. [[CrossRef](#)]
43. ED Chaves, M.; CA Picoli, M.; D Sanches, I. Recent applications of Landsat 8/OLI and Sentinel-2/MSI for land use and land cover mapping: A systematic review. *Remote Sens.* **2020**, *12*, 3062. [[CrossRef](#)]
44. Leta, M.K.; Demissie, T.A.; Tränckner, J. Modeling and prediction of land use land cover change dynamics based on land change modeler (LCM) in Nashe watershed, Upper Blue Nile basin, Ethiopia. *Sustainability* **2021**, *13*, 3740. [[CrossRef](#)]
45. Moncrieff, G.R. Continuous land cover change detection in a critically endangered shrubland ecosystem using neural networks. *Remote Sens.* **2022**, *14*, 2766. [[CrossRef](#)]
46. Yan, J.; Wang, L.; He, H.; Liang, D.; Song, W.; Han, W. Large-area land-cover changes monitoring with time-series remote sensing images using transferable deep models. *IEEE Trans. Geosci. Remote* **2022**, *60*, 1–17. [[CrossRef](#)]
47. Temgoua, L.F.; Meyabeme Elono, A.L.; Mfonkwet Njiaghait, Y.; Ngouh, A.; Nzuta Kengne, C. Land use and land cover dynamics in the Melap Forest Reserve, West Cameroon: Implications for sustainable management. *Geol. Ecol. landsc.* **2022**, *6*, 305–315. [[CrossRef](#)]
48. Faruque, M.J.; Vekerdy, Z.; Hasan, M.Y.; Islam, K.Z.; Young, B.; Ahmed, M.T.; Shovon, S.M.; Kakon, F.J.; Kundu, P. Monitoring of land use and land cover changes by using remote sensing and GIS techniques at human-induced mangrove forests areas in Bangladesh. *Remote Sens. App Soc. Environ.* **2022**, *25*, 100699. [[CrossRef](#)]
49. Kombate, A.; Folega, F.; Atakpama, W.; Dourma, M.; Wala, K.; Goïta, K. Characterization of land-cover changes and forest-cover dynamics in Togo between 1985 and 2020 from Landsat images using Google Earth Engine. *Land* **2022**, *11*, 1889. [[CrossRef](#)]
50. Souverijns, N.; Buchhorn, M.; Horion, S.; Fensholt, R.; Verbeeck, H.; Verbesselt, J.; Herold, M.; Tsendbazar, N.-E.; Bernardino, P.N.; Somers, B.; et al. Thirty years of land cover and fraction cover changes over the Sudano-Sahel using Landsat time series. *Remote Sens.* **2020**, *12*, 3817. [[CrossRef](#)]
51. Dibaba, W.T.; Demissie, T.A.; Miegel, K. Drivers and implications of land use/land cover dynamics in Finchaa Catchment, Northwestern Ethiopia. *Land* **2020**, *9*, 113. [[CrossRef](#)]
52. Mugo, R.; Waswa, R.; Nyaga, J.W.; Ndubi, A.; Adams, E.C.; Flores-Anderson, A.I. Quantifying land use land cover changes in the Lake Victoria basin using satellite remote sensing: The trends and drivers between 1985 and 2014. *Remote Sens.* **2020**, *12*, 2829. [[CrossRef](#)]
53. Feng, S.; Li, W.; Xu, J.; Liang, T.; Ma, X.; Wang, W.; Yu, H. Land use/Land cover mapping based on GEE for the monitoring of changes in ecosystem types in the upper Yellow River Basin over the Tibetan Plateau. *Remote Sens.* **2022**, *14*, 5361. [[CrossRef](#)]
54. Zhang, Y.; Wang, J.; Wang, Y.; Ochir, A.; Togtokh, C. Land cover change analysis to assess sustainability of development in the Mongolian Plateau over 30 years. *Sustainability* **2022**, *14*, 6129. [[CrossRef](#)]
55. Jiang, W.; Fu, B.; Lü, Y. Assessing impacts of land use/land cover conversion on changes in ecosystem services value on the Loess Plateau, China. *Sustainability* **2020**, *12*, 7128. [[CrossRef](#)]
56. Du, X.; Zhao, X.; Liang, S.; Zhao, J.; Xu, P.; Wu, D. Quantitatively assessing and attributing land use and land cover changes on China's Loess Plateau. *Remote Sens.* **2020**, *12*, 353. [[CrossRef](#)]
57. Liu, C.; Li, W.; Zhu, G.; Zhou, H.; Yan, H.; Xue, P. Land use/Land cover changes and their driving factors in the Northeastern Tibetan Plateau based on geographical detectors and Google Earth Engine: A case study in Gannan Prefecture. *Remote Sens.* **2020**, *12*, 3139. [[CrossRef](#)]
58. Moumane, A.; Al Karkouri, J.; Benmansour, A.; El Ghazali, F.E.; Fico, J.; Karmaoui, A.; Batchi, M. Monitoring long-term land use, land cover change, and desertification in the Ternata oasis, Middle Draa Valley, Morocco. *Remote Sens. App Soc. Environ.* **2022**, *26*, 100745. [[CrossRef](#)]
59. Thamaga, K.H.; Dube, T.; Shoko, C. Evaluating the impact of land use and land cover change on unprotected wetland ecosystems in the arid-tropical areas of South Africa using the Landsat dataset and support vector machine. *Geocarto Int.* **2022**, *37*, 10344–10365. [[CrossRef](#)]
60. Baeza, S.; Paruelo, J.M. Land use/Land cover change (2000–2014) in the Rio de la Plata grasslands: An analysis based on MODIS NDVI time series. *Remote Sens.* **2020**, *12*, 381. [[CrossRef](#)]
61. Gozdowski, D.; Žukovskis, J.; Razinkovas-Baziukas, A.; Wójcik-Gront, E. Land cover changes in selected areas next to lagoons located on the southern coast of the Baltic Sea, 1984–2021. *Sustainability* **2022**, *14*, 2006. [[CrossRef](#)]
62. Nasiri, V.; Deljouei, A.; Moradi, F.; Sadeghi, S.M.M.; Borz, S.A. Land use and Land cover mapping using Sentinel-2, Landsat-8 satellite images, and google earth engine: A comparison of two composition methods. *Remote Sens.* **2022**, *14*, 1977. [[CrossRef](#)]
63. Som-ard, J.; Immitzer, M.; Vuolo, F.; Ninsawat, S.; Atzberger, C. Mapping of crop types in 1989, 1999, 2009 and 2019 to assess major land cover trends of the Udorn Thani Province, Thailand. *Comput. Electron. Agric.* **2022**, *198*, 107083. [[CrossRef](#)]
64. Xu, L.; Herold, M.; Tsendbazar, N.E.; Masiliūnas, D.; Li, L.; Lesiv, M.; Fritz, S.; Verbesselt, J. Time series analysis for global land cover change monitoring: A comparison across sensors. *Remote Sens. Environ.* **2022**, *271*, 112905. [[CrossRef](#)]
65. Deng, X.; Jiang, Q.O.; Zhan, J.; He, S.; Lin, Y. Simulation on the dynamics of forest area changes in Northeast China. *J. Geogr. Sci.* **2010**, *20*, 495–509. [[CrossRef](#)]

66. Devi, A.B.; Deka, D.; Aneesh, T.D.; Srinivas, R.; Nair, A.M. Predictive modelling of land use land cover dynamics for a tropical coastal urban city in Kerala, India. *Arab. J. Geosci.* **2022**, *15*, 399. [CrossRef]
67. Faichia, C.; Tong, Z.; Zhang, J.; Liu, X.; Kazuva, E.; Ullah, K.; Al-Shaibah, B. Using RS data-based CA-Markov model for dynamic simulation of historical and future LUCC in Vientiane, Laos. *Sustainability* **2020**, *12*, 8410. [CrossRef]
68. Nath, N.; Sahariah, D.; Meraj, G.; Debnath, J.; Kumar, P.; Lahon, D.; Chand, K.; Farooq, M.; Chandan, P.; Singh, S.K.; et al. Land use and land cover change monitoring and prediction of a UNESCO world heritage site: Kaziranga eco-sensitive zone using Cellular Automata-Markov Model. *Land* **2023**, *12*, 151. [CrossRef]
69. Liu, S.; Deng, J. The range suitable for GM (1,1). *Syst. Eng. Theory Pract.* **2000**, *5*, 121–124.
70. Zhou, L.; Wang, S.; Du, M.; Yang, J.; Zhu, Y.; Wu, J. An integrated approach for detection and prediction of greening situation in a typical desert area in China and its human and climatic factors analysis. *ISPRS Int. J. Geo-Inf.* **2020**, *9*, 364. [CrossRef]
71. Xie, N.; Wang, R. A historic review of grey forecasting models. *J. Grey Syst.* **2017**, *29*, 1–29.
72. Zhang, X.; Bao, J.; Xu, S.; Wang, Y.; Wang, S. Prediction of China's grain consumption from the perspective of sustainable development—Based on GM(1,1) model. *Sustainability* **2022**, *14*, 10792. [CrossRef]
73. Tan, X.; Xu, J.; Li, F.; Wu, M.; Chen, D.; Liang, Y. Improved GM (1,1) model by optimizing initial condition to predict satellite clock bias. *Math. Probl. Eng.* **2022**, *2022*, 3895884. [CrossRef]
74. Zhang, X.; Wu, X.; Xiao, Y.; Shi, J.; Zhao, Y.; Zhang, M. Application of improved seasonal GM (1,1) model based on HP filter for runoff prediction in Xiangjiang River. *Environ. Sci. Pollut. R.* **2022**, *29*, 52806–52817. [CrossRef]
75. Zhao, Y.; Feng, D.; Yu, L.; Cheng, Y.; Zhang, M.; Liu, X.; Xu, Y.; Fang, L.; Zhu, Z.; Gong, P. Long-term land cover dynamics (1986–2016) of Northeast China derived from a multi-temporal Landsat archive. *Remote Sens.* **2019**, *11*, 599. [CrossRef]
76. Wang, H.; Yang, S.; Wang, Y.; Wang, Y.; Gu, Z.; Xiong, S.; Huang, H.; Sun, M.; Zhang, S.; Guo, L.; et al. Rates and causes of black soil erosion in Northeast China. *Catena* **2022**, *214*, 106250. [CrossRef]
77. Yao, Q.; Liu, J.; Yu, Z.; Li, Y.; Jin, J.; Liu, X.; Wang, G. Three years of biochar amendment alters soil physiochemical properties and fungal community composition in a black soil of northeast China. *Soil Biol. Biochem.* **2017**, *110*, 56–67. [CrossRef]
78. Wang, Q.; Guo, P.; Dong, S.; Liu, Y.; Pan, Y.; Li, C. Extraction of cropland spatial distribution information using multi-Seasonal fractal features: A case study of black soil in Lishu County, China. *Agriculture* **2023**, *13*, 486. [CrossRef]
79. Zhang, B.; Cui, H.; Yu, L.; He, Y. Land reclamation process in Northeast China since 1900. *Chinese Geogr. Sci.* **2003**, *13*, 119–123. [CrossRef]
80. Deng, X.; Jiang, Q.; Su, H.; Wu, F. Trace forest conversions in Northeast China with a 1-km area percentage data model. *J. Appl. Remote Sens.* **2010**, *4*, 041893. [CrossRef]
81. Liu, Z.; Wang, W.J.; Ballantyne, A.; He, H.S.; Wang, X.; Liu, S.; Ciais, P.; Wimberly, M.C.; Piao, S.; Yu, K.; et al. Forest disturbance decreased in China from 1986 to 2020 despite regional variations. *Commun. Earth Environ.* **2023**, *4*, 15. [CrossRef]
82. Ye, Y.; Fang, X.; Ren, Y.; Zhang, X.; Li, C. Cropland cover change in Northeast China during the past 300 years. *Sci. China Ser. D-Earth Sci.* **2009**, *52*, 1172–1182. [CrossRef]
83. Mao, D.; He, X.; Wang, Z.; Tian, Y.; Xiang, H.; Yu, H.; Ma, W.; Jia, M.; Ren, C.; Zheng, H. Diverse policies leading to contrasting impacts on land cover and ecosystem services in Northeast China. *J. Clean. Prod.* **2019**, *240*, 117961. [CrossRef]
84. Liu, S.; Wang, D.; Li, H.; Li, W.; Wu, W.; Zhu, Y. The Ecological security pattern and its constraint on urban expansion of a black soil farming area in Northeast China. *ISPRS Int. J. Geo-Inf.* **2017**, *6*, 263. [CrossRef]
85. Xie, Y.; Lin, H.; Ye, Y.; Ren, X. Changes in soil erosion in cropland in northeastern China over the past 300 years. *Catena* **2019**, *176*, 410–418. [CrossRef]
86. Zhu, B.; Zhu, X.; Zhang, R.; Zhao, X. Study of multiple land use planning based on the coordinated development of wetland farmland: A case study of Fuyuan City, China. *Sustainability* **2019**, *11*, 271. [CrossRef]
87. Liu, B.; Zhang, G.; Xie, Y.; Shen, B.; Gu, Z.; Ding, Y. Delineating the black soil region and typical black soil region of northeastern China. *Chin. Sci. Bull.* **2021**, *66*, 96–106. [CrossRef]
88. Gorelick, N.; Hancher, M.; Dixon, M.; Ilyushchenko, S.; Thau, D.; Moore, R. Google Earth Engine: Planetary-scale geospatial analysis for everyone. *Remote Sens. Environ.* **2017**, *202*, 18–27. [CrossRef]
89. Zhang, X.; Liu, L.; Chen, X.; Gao, Y.; Xie, S.; Mi, J. GLC_FCS30: Global land-cover product with fine classification system at 30 m using time-series Landsat imagery. *Earth Syst. Sci. Data* **2021**, *13*, 2753–2776. [CrossRef]
90. Liu, L.; Zhang, X.; Gao, Y.; Chen, X.; Shuai, X.; Mi, J. Finer-resolution mapping of global land cover: Recent developments, consistency analysis, and prospects. *J. Remote Sens.* **2021**, *2021*, 5289697. [CrossRef]
91. Qiao, Q.; Zhen, Z.; Liu, L.; Luo, P. The construction of ecological security pattern under rapid urbanization in the Loess Plateau: A case study of Taiyuan City. *Remote Sens.* **2023**, *15*, 1523. [CrossRef]
92. Peskun, P.H. Guidelines for choosing the transition matrix in Monte Carlo methods using Markov chains. *J. Comput. Phys.* **1981**, *40*, 327–344. [CrossRef]
93. Sherlaw-Johnson, C.; Gallivan, S.; Burridge, J. Estimating a Markov transition matrix from observational data. *J. Oper. Res. Soc.* **1995**, *46*, 405–410. [CrossRef]
94. Bickenbach, F.; Bode, E. Markov or not Markov—This should be a question. *Kiel Work. Pap.* **2001**, *1086*, 1–28. Available online: <http://hdl.handle.net/10419/2673> (accessed on 6 July 2023).
95. Ma, D.; Zhao, S. Quantitative analysis of land subsidence and its effect on vegetation in Xishan Coalfield of Shanxi Province. *ISPRS Int. J. Geoinf.* **2022**, *11*, 154. [CrossRef]

96. Liu, B.; Zhang, G.; Xie, Y.; Shen, B.; Gu, Z.; Ding, Y. Boundary dataset of black and typical black soil regions in Northeast China. *Digit. J. Glob. Change Data Repos.* 2021.
97. Xing, H.; Wang, H.; Zhang, J.; Hou, D. Monitoring land cover change by leveraging a dynamic service-oriented computing model. *Remote Sens.* **2023**, *15*, 736. [[CrossRef](#)]
98. Hoque, M.Z.; Ahmed, M.; Islam, I.; Cui, S.; Xu, L.; Prodhon, F.A.; Ahmed, S.; Rahman, M.A.; Hasan, J. Monitoring changes in land use land cover and ecosystem service values of dynamic saltwater and freshwater systems in coastal Bangladesh by geospatial techniques. *Water* **2022**, *14*, 2293. [[CrossRef](#)]
99. Debnath, J.; Sahariah, D.; Lahon, D.; Nath, N.; Chand, K.; Meraj, G.; Singh, S.K. Geospatial modeling to assess the past and future land use-land cover changes in the Brahmaputra Valley, NE India, for sustainable land resource management. *Environ. Sci. Pollut. Res.* **2022**, *24248*, 1–24. [[CrossRef](#)]
100. Dhanaraj, K.; Angadi, D.P. Land use land cover mapping and monitoring urban growth using remote sensing and GIS techniques in Mangaluru, India. *GeoJournal* **2022**, *87*, 1133–1159. [[CrossRef](#)]
101. Das, S.; Angadi, D.P. Land use land cover change detection and monitoring of urban growth using remote sensing and GIS techniques: A micro-level study. *GeoJournal* **2022**, *87*, 2101–2123. [[CrossRef](#)]
102. Çağlıyan, A.; Dağlı, D. Monitoring land use land cover changes and modelling of urban growth using a future land use simulation model (FLUS) in Diyarbakır, Turkey. *Sustainability* **2022**, *14*, 9180. [[CrossRef](#)]
103. Li, Q.; Wang, L.; Du, G.; Faye, B.; Li, Y.; Li, J.; Liu, W.; Qu, S. Dynamic variation of ecosystem services value under land use/cover change in the black soil region of Northeastern China. *Int. J. Environ. Res. Public Health* **2022**, *19*, 7533. [[CrossRef](#)] [[PubMed](#)]
104. Wang, H.; Zhang, C.; Yao, X.; Yun, W.; Ma, J.; Gao, L.; Li, P. Scenario simulation of the trade off between ecological land and farmland in black soil region of Northeast China. *Land Use Policy* **2022**, *114*, 105991. [[CrossRef](#)]
105. Ray, R.; Das, A.; Hasan, M.S.U.; Aldrees, A.; Islam, S.; Khan, M.A.; Lama, G.F.C. Quantitative analysis of land use and land cover dynamics using geoinformatics techniques: A case study on Kolkata metropolitan development authority (KMDA) in West Bengal, India. *Remote Sens.* **2023**, *15*, 959. [[CrossRef](#)]
106. Zou, X.; Liu, X.; Liu, M.; Tian, L.; Zhu, L.; Zhang, Q. Spatiotemporal graph-based analysis of land cover evolution using remote sensing time series data. *Int. J. Geogr. Inf. Sci.* **2023**, *37*, 1009–1040. [[CrossRef](#)]
107. Wang, J.; Wang, Z.; Cheng, H.; Kang, J.; Liu, X. Land cover changing pattern in pre-and post-earthquake affected area from remote sensing data: A case of Lushan County, Sichuan Province. *Land* **2022**, *11*, 1205. [[CrossRef](#)]
108. Wang, Q.; Wang, H.; Chang, R.; Zeng, H.; Bai, X. Dynamic simulation patterns and spatiotemporal analysis of land-use/land-cover changes in the Wuhan metropolitan area, China. *Ecol. Model.* **2022**, *464*, 109850. [[CrossRef](#)]
109. Mwabumba, M.; Yadav, B.K.; Rwiza, M.J.; Larbi, I.; Twisa, S. Analysis of land use and land-cover pattern to monitor dynamics of Ngorongoro world heritage site (Tanzania) using hybrid cellular automata-Markov model. *Curr. Res. Env. Sust.* **2022**, *4*, 100126. [[CrossRef](#)]
110. Li, K.; Feng, M.; Biswas, A.; Su, H.; Niu, Y.; Cao, J. Driving factors and future prediction of land use and cover change based on satellite remote sensing data by the LCM model: A case study from Gansu Province, China. *Sensors* **2020**, *20*, 2757. [[CrossRef](#)]
111. Singh, B.; Venkatramanan, V.; Deshmukh, B. Monitoring of land use land cover dynamics and prediction of urban growth using Land Change Modeler in Delhi and its environs, India. *Environ. Sci. Pollut. Res.* **2022**, *29*, 71534–71554. [[CrossRef](#)] [[PubMed](#)]
112. Jiao, M.; Hu, M.; Xia, B. Spatiotemporal dynamic simulation of land-use and landscape-pattern in the Pearl River Delta, China. *Sustain. Cities Soc.* **2019**, *49*, 101581. [[CrossRef](#)]
113. Rao, Y.; Zhou, M.; Ou, G.; Dai, D.; Zhang, L.; Zhang, Z.; Nie, X.; Yang, C. Integrating ecosystem services value for sustainable land-use management in semi-arid region. *J. Clean Prod.* **2018**, *186*, 662–672. [[CrossRef](#)]
114. Wang, S.; Xu, X.; Huang, L. Spatial and temporal variability of soil erosion in Northeast China from 2000 to 2020. *Remote Sens.* **2023**, *15*, 225. [[CrossRef](#)]
115. Zhang, T.; Sun, F.; Lei, Q.; Jiang, Z.; Luo, J.; Lindsey, S.; Liu, H. Quantification of soil element changes in long-term agriculture: A case study in Northeast China. *Catena* **2022**, *208*, 105766. [[CrossRef](#)]
116. Yan, X.; An, J.; Yin, Y.; Gao, C.; Wang, B.; Wei, S. Heavy metals uptake and translocation of typical wetland plants and their ecological effects on the coastal soil of a contaminated bay in Northeast China. *Sci. Total Environ.* **2022**, *803*, 149871. [[CrossRef](#)] [[PubMed](#)]

Disclaimer/Publisher’s Note: The statements, opinions and data contained in all publications are solely those of the individual author(s) and contributor(s) and not of MDPI and/or the editor(s). MDPI and/or the editor(s) disclaim responsibility for any injury to people or property resulting from any ideas, methods, instructions or products referred to in the content.